Influence of activating fluxes on weld bead geometry, microstructures and mechanical properties of IRSM 41 A-TIG weldments

P. Sivateja*, R. S. Vidyarthy

BITS-Pilani, Hyderabad Campus, Telangana, India

Presented in International Conference on Precision, Micro, Meso and Nano Engineering (COPEN - 12: 2022)
December 8th - 10th, 2022 IIT Kanpur, India

KEYWORDS

IRSM 41,
A-TIG,
Weld Bead Geometry,
Microstructures,
Hardness.

ABSTRACT

IRSM 41 is a corrosion-resistant steel widely employed in railway wagons. In the present study, IRSM 41 steel plates of 8 mm thickness were joined using conventional TIG welding (C-TIG) and activated tungsten inert gas welding (A-TIG). Three multicomponent fluxes were utilised during the A-TIG welding. The application of fluxes enhanced the depth of penetration and reduced the bead width. Weldments produced with flux 3 have a thorough penetration of 8 mm in a single weld pass. Bead geometry has been analysed through various aspects such as bead width, depth of penetration and depth-to-width ratio. Metallographic examination and Hardness study of C-TIG and A-TIG weldments was performed. The average fusion zone hardness was found to be better in A-TIG weldments than in C-TIG weldments. The obtained weldments bead geometry and properties have been discussed in contrast of various input parameters.

1. Introduction

IRSM 41 steel is a corten steel that exhibits enhanced atmospheric corrosion resistance (Deepak et al., 2021). It is widely used in railway wagons, auto-mobile, highway buildings, tower buildings, bridge buildings and Photovoltaic power stations because of its improved corrosion properties (Deepak et al., 2019; Dong et al., 2018). Alloying elements such as chromium, copper, silicon and phosphorous in IRSM 41 enhance the corrosion resistance (Raj et al., 2020). Besides this, IRSM 41 exhibits high strength, good durability, high-temperature resistance, and long service life (Hafez et al., 2017). For the fabrication of IRSM 41 steel components, various techniques, namely welding, bolting, and riveting, are regularly used. Amongst them, welding is most commonly used.

Welding of IRSM 41 is significantly influenced by welding procedure and chemical composition. Low carbon and a smaller proportion of alloying elements in IRSM 41 attribute to good weldability. Arc welding processes are regularly used for the joining of IRSM 41 sheets (Beeharry & Surnam, 2018). Among various arc welding techniques, Tungsten inert gas welding (TIG) is extensively utilised because of its good weld quality, surface appearance, and low operational costs. However, achieving full penetration in a single weld pass is difficult, resulting in lower productivity in conventional TIG welding (C-TIG). To resolve the lower penetration issue, a new method known as A-TIG welding is used. In this method, activating fluxes are coated over the plate surface before C-TIG welding. Initially, fluxes were used to reduce porosity. However, several researchers Rana et al. (2021); Sivakumar et al. (2021); Vidyarthy and Sivateja (2020) observed that fluxes have a considerable effect on weld penetration and mechanical properties. Vasudevan (2017) analysed the influence of fluxes on weld geometry, microstructure and mechanical properties during A-TIG welding. The researcher observed that A-TIG weldments had enhanced penetration compared to C-TIG weldments. A thorough penetration of 10 mm on 304 LN and 12 mm on 316 LN was attained in a single weld pass during A-TIG welding. Furthermore, the microstructural and mechanical properties of A-TIG weldments were noticed to be better than base metal and C-TIG weldments (Sharma & Dwivedi, 2019).

Although A-TIG welding has recently been widely used for joining various steels, the research works

*Corresponding author
E-mail: p20190045@hyderabad.bits-pilani.ac.in

https://doi.org/10.58368/MTT.22.1.2023.7-12

reported on the A-TIG welding of IRSM 41 are very limited. The influence of activating fluxes employed during A-TIG of IRSM 41 on weld geometry and mechanical properties are not widely explored. So, in the present work, three multicomponent fluxes were used during A-TIG welding of IRSM 41 plates of 8 mm thickness, and their influences on the weld geometry, microstructure and hardness have been investigated. Subsequently, a correlation was established amongst welding parameters and the weld quality.

2. Materials and Methods

2.1. Base metal

In the current work, an IRSM 41 steel plate having a thickness of 8 mm is used as a base material. Carbon and alloying elements such as chromium, silicon, manganese, nickel, titanium, aluminium, phosphorus, and sulphur are present in the base metal. The chemical composition of the base metal is C (0.08 wt.%), Mn (0.38 wt.%), Si (0.29 wt.%), Cr (0.53), Al (0.01 wt.%), P (0.05 wt.%), S (0.05 wt.%), Ti (0.05 wt.%), Ni (0.22 wt.%). The mechanical properties of IRSM 41 steel are presented in Table 1. The base metal microstructure (Figure 1) showing two phases, ferrite and pearlite. The proportion of ferrite (light phases) is found considerably more compared to the pearlite (light phases). Homogenous distribution of ferrite and pearlite phases was observed in the base material.

Table 1
Mechanical properties of IRSM 41.

Grade	Tensile strength (MPa)	Yield stress (offset 0.2 %) (MPA)	Hardness (VHN)
IRSM 41	440 ± 2.95	340 ± 5	159 ± 7

2.2. Welding procedure

IRSM 41 plates with dimensions 150*110*8 mm^3 were extracted by wire EDM and used as substrate for bead-on plates welding. The extracted plates were grinded, polished and thoroughly cleaned with acetone before welding. Tungsten inert gas welding was conducted with and without the fluxes. Three different multicomponent fluxes containing oxide fluxes with varying weight proportions were prepared for A-TIG welding. The fluxes were applied on the surface by means of a paintbrush. The coating density of applied fluxes was observed to be around 2-3 mg/cm^2. The welding was conducted with a direct current electrode negative (DCEN) power source. A speed of 80 mm/min and a current of 220 A was maintained during the welding. The gap between the workpiece and the electrode tip was about 3.2mm. Pure argon gas was provided at a rate of 10 LPM for shielding the weld region.

2.3. Characterisation techniques

After welding, the weld joint was examined visually to find the existence of surface imperfections such as surface cracks, incomplete fusion and porosity. Samples were extracted transversely from the defect-free weld joints for mechanical and metallographic examination. Mechanical polishing was performed on the extracted samples with silicon carbide emery papers possessing grit sizes varying from 100 to 2000. After that, the samples underwent cloth polishing by using aqueous alumina powder. Vilella's reagent (5 ml Hydrochloric acid + 1 g Picric Acid + 100 ml Ethanol) was used for etching the polished samples.

Macroscopic analysis was carried out by examining the etched specimens using a stereomicroscope. An inverted microscope (Make: Meiji Techno,

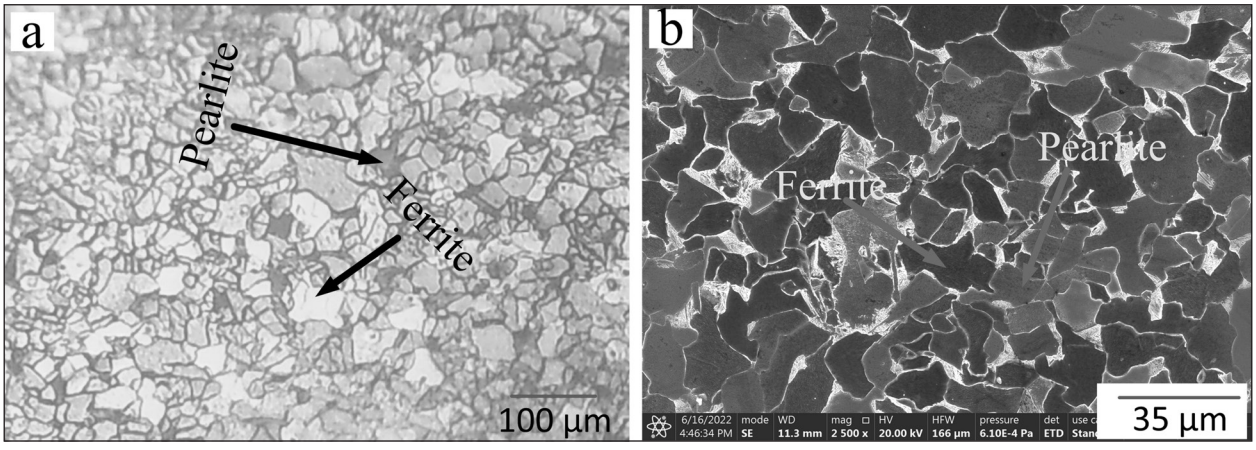

Fig. 1. Microstructure of IRSM 41 steel at (a) lower magnification and (b) higher magnification.

Model: IM7200) and field emission scanning electron microscope (FESEM) (Make: FEI, Model: Apreo LoVac) was used to investigate the microstructures acquired at various zones (base metal, HAZ, FZ) of A-TIG and C-TIG weldments. The mechanical characterisation of A-TIG and C-TIG weldments was carried out by evaluating the Vickers hardness. During the hardness testing, a 200 g load was supplied for 10 s dwell time in the microhardness tester (Make: Mitutoyo, Model: HM-200). The readings were recorded at regular intervals of 0.5 mm.

3. Results and Discussion

3.1. Macroscopic analysis

The cross-section of the weldments produced with A-TIG and C-TIG are shown in Figure 2 (a-d). The weld bead geometry has been analysed through various factors such as bead width, depth of penetration and depth-to-width ratio, as presented in Figure 3. The weld bead width and depth of penetration of C-TIG weldments were 13 ± 0.5 mm and 2.5 ± 0.1 mm, respectively (Figure 3). It was noticed that usage of fluxes during A-TIG welding contributes to an improved weld penetration and depth-to-width ratio in all cases. For the weldments produced with flux 3, a thorough penetration of 8 mm was attained in a single pass. Depth of penetration of 6.07 ± 0.1 mm and 7.46 ± 0.1 mm was witnessed in flux 1 and flux 2 weldments. The weld bead width corresponding to flux 1, flux 2, and flux 3 were 11 ± 0.4 mm, 10.07 ± 0.4 mm, and 9.21 ± 0.5 mm, respectively. Among all the weldments, flux 3 produced full penetration with lower bead width. Therefore, C-TIG and flux 3 weldments were used for further analysis.

The improved penetration in A-TIG weldments was mainly because of two mechanisms reversal Marangoni convection and arc constriction (Mills et al., 1998). In C-TIG weldments, the weld centre experiences lower surface tension and higher temperature. Contrarily the weld periphery exhibits higher surface tension and lower temperature. Because of the negative surface tension gradient, the molten metal flows radially outwards, leading to a shallow and wider weld geometry Kulkarni et al., (2019); Unni & Muthukumaran, (2021). On the other hand, in A-TIG welding, flux application alters the behaviour of surface tension with temperature. So, the weld periphery experiences lower surface tension, and higher surface tension was witnessed at the weld centre. Because of the positive surface tension gradient, molten liquid flows from the weld periphery to the weld centre, producing a narrower and deeper weld geometry (Pavan et al., 2021). Arc constriction is the other mechanism which increases the weld penetration. The activating flux applied gets vaporised because of the heat generated during the welding. The vaporised flux disassociates into elements and produces a vapour cover surrounding the arc column. The vapour covers absorb the electron from the outer periphery of the arc, causing an arc constriction.The constricted arc decreases the anode spot area, causing an enhancement in current density. Higher current densities generated produce deeper and narrower weld beads (Vidyarthy et al., 2018).

3.2. Microstructural analysis

Optical and FE-SEM microstructures acquired at the fusion zone (FZ) heat-affected zone (HAZ) and of flux 3 and C-TIG weldments are shown in Figure 4 (a-h). Weld fusion zone of flux 3 weldments (Figure 4 (a, b)) principally contains martensite, widmanstatten ferrite (WF), and grain boundary ferrite. Similar microstructural phases were witnessed in the C-TIG weldment fusion zone

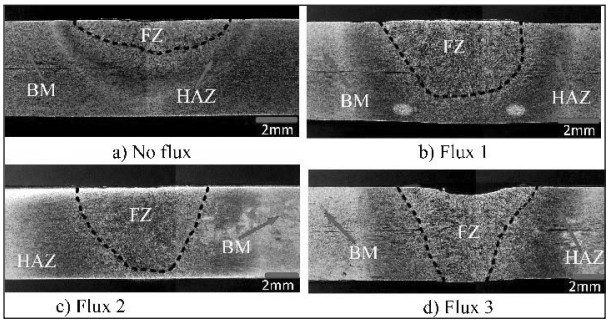

Fig. 2. Macrostructures of the weldments produced in different conditions.

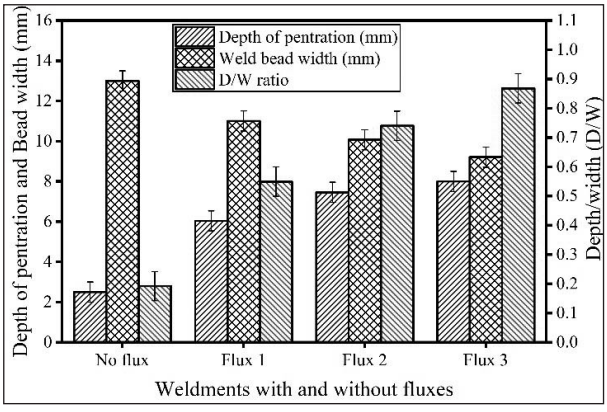

Fig. 3. Variation of weld bead width, weld penetration, depth-to-width ratio of the weldments produced with and without fluxes.

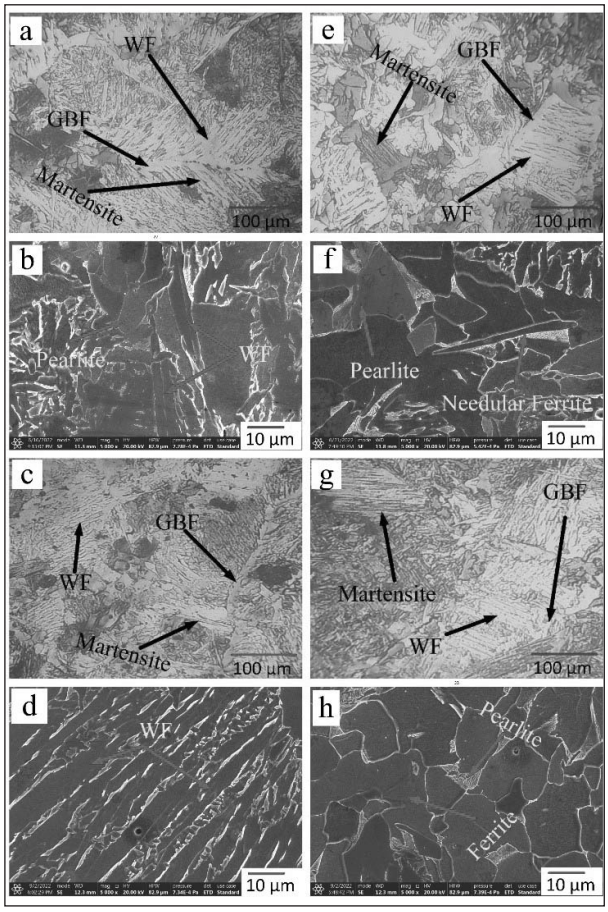

Fig. 4. Optical and FE-SEM microstructures of flux 3 weldments showing (a & b) fusion zone, (e & f) HAZ; Optical and FE-SEM microstructures of C-TIG weldments showing (c & d) fusion zone, (g & h) HAZ.

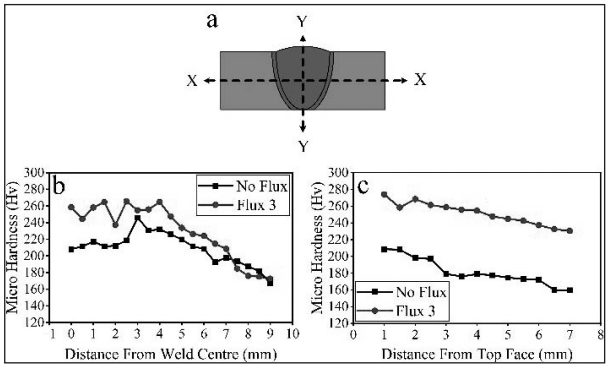

Fig. 5. Schematics show (a) hardness testing pattern, (b) hardness profile across X-X direction and (c) hardness across Y-Y direction.

(Figure 4 (c, d)). Since the fusion zone experiences higher temperatures, more ferritic to austenitic transformation takes place. Due to considerable austenitic formation, the martensite formed during the cooling of austenite was significantly high. Hence, a more proportion of martensite was observed in the fusion zone (Suryana et al., 2019). Widmanstatten ferrite generated has a needle structure, and they are developed epitaxially or within the boundary. Further, HAZ of both C-TIG (Figure 4 (g, h)) and flux 3 weldments (Figure 4 (e, f)) consists of widmanstatten ferrite (WF), grain boundary ferrite (GB), martensite and pearlite. Temperatures in HAZ are marginally higher than Ac1 temperature (724 °C). At this temperature range, coarsening of ferrite and pearlite is more predominant. In addition to this, a smaller proportion of ferritic to austenitic transformation also occurs. Due to lower austenitic transformation, the martensite formed from the austenite is less. Hence, a lower proportion of martensite was observed in HAZ.

3.3. Hardness analysis

Hardness values of the weldments were acquired along X and Y directions, and the same is shown in Figure 5a. The hardness distribution from the fusion zone towards the base metal in C-TIG and flux 3 weldments is presented in Figure 5b. In both weldments, the hardness profile followed a decremental path from the fusion zone towards the base metal. The Average hardness of the base metal, HAZ and fusion zone for C-TIG and flux 3 weldments are shown in Table 2. For both C-TIG and flux 3 weldments, the fusion zone's average hardness was higher than the HAZ and base metal. The existence of martensite and widmanstatten ferrite may contribute to the fusion zone's enhanced hardness. HAZ of both the weldments has superior hardness than the base metal. The increased hardness in HAZ was may be due to the presence of widmanstatten ferrite and a lower proportion of martensite. Furthermore, while measuring the hardness from the top face to the root face (shown in Figure 5c), a significant variation in hardness was witnessed in the fusion zone.

Table 2
Average hardness (Hv) across various zones for C-TIG and flux 3 weldments.

Weldments	Average hardness (Hv) across various zones		
	FZ	HAZ	Base metal
C-TIG	221 ± 24	200.8 ± 8	176.7 ± 5
Flux 3	255 ± 10	221.3 ± 12	177 ± 5

4. Conclusions

In the current work, A-TIG welding was conducted on 8 mm thick IRSM 41 bead on plates with and without the application of fluxes. Based on metallographic and hardness analysis, the following conclusions were made

- Application of fluxes significantly increased the weld penetration and depth-to-width ratio. More than 320 % enhancement in weld penetration was observed in A-TIG in comparison with C-TIG weldments.
- An 8 mm complete penetration was attained in a single weld pass by applying flux 3 during A-TIG of IRSM 41 steel.
- Microstructural analysis reveals the existence of martensite, widmanstatten ferrite (W), and grain boundary ferrite in the fusion zone of all the weldments. Heat affected zone consists of WF, GBF, pearlite and ferrite.
- Hardness study reveals that fusion zone of all the weldments exhibits higher hardness than the HAZ and base metal. The enhanced hardness was resulted due to the presence of martensite and WF.

References

Beeharry, P., & Surnam, B. Y. R. (2018). Atmospheric Corrosion of Welded Mild Steel. *Materials Today: Proceedings*, *5*(2), 7476-7485. https://doi.org/10.1016/j.matpr.2017.11.419

Deepak, J. R., Bupesh Raja, V. K., & Kaliaraj, G. S. (2019). Mechanical and corrosion behavior of Cu, Cr, Ni and Zn electroplating on corten A588 steel for scope for betterment in ambient construction applications. *Results in Physics*, *14*(June), 102437. https://doi.org/10.1016/j.rinp.2019.102437

Deepak, J. R., Bupesh Raja, V. K., Kavitha, K. R., Giresh Reddy, K., & Venkat, M. (2021). Microstructure and metallurgical property investigation of welded IRSM 41-97 rail steel joints. *Materials Today: Proceedings*, *47*(xxxx), 4827-4832. https://doi.org/10.1016/j.matpr.2021.06.056

Dong, C., Zhao, A. min, Wang, X. tao, Pang, Q. hang, & Wu, H. bin. (2018). Microstructure and properties of 1100 MPa grade low-carbon hot-rolled steel by laser welding. *Journal of Iron and Steel Research International*, *25*(2). https://doi.org/10.1007/s42243-018-0025-3

Hafez, K. M., Ramadan, M., Fathy, N., & Ismail, M. (2017). Microstructure and mechanical properties of laser welded dual phase and mild steel joints for automotive applications. *Applied Mechanics and Materials*, *865*. https://doi.org/10.4028/www.scientific.net/amm.865.81

Kulkarni, A., Dwivedi, D. K., & Vasudevan, M. (2019). Dissimilar metal welding of P91 steel-AISI 316L SS with Incoloy 800 and Inconel 600 interlayers by using activated TIG welding process and its effect on the microstructure and mechanical properties. *Journal of Materials Processing Technology*, *274*, 1-13. https://doi.org/10.1016/j.jmatprotec.2019.116280

Mills, K. C., Keene, B. J., Brooks, R. F., & Shirali, A. (1998). Marangoni effects in welding. *Philosophical Transactions of the Royal Society A: Mathematical, Physical and Engineering Sciences*, *356*(1739), 911-925. https://doi.org/10.1098/rsta.1998.0196

Pavan, A. R., Chandrasekar, N., Arivazhagan, B., Kumar, S., & Vasudevan, M. (2021). Study of arc characteristics using varying shielding gas and optimization of activated-tig welding technique for thick AISI 316L(N) plates. *CIRP Journal of Manufacturing Science and Technology*, *35*. https://doi.org/10.1016/j.cirpj.2021.08.013

Raj, D. J., Raja, V. K. B., Joy, N., Nikesh, P., & Ujjwal, P. K. (2020). FEA and micro structural investigation of autogenous GTAW and laser beam weld IRSM 41-97 steel joints. *AIP Conference Proceedings*, *2311*. https://doi.org/10.1063/5.0034615

Rana, H., Badheka, V., Patel, P., Patel, V., Li, W., & Andersson, J. (2021). Augmentation of weld penetration by flux assisted TIG welding and its distinct variants for oxygen free copper. *Journal of Materials Research and Technology*, *10*. https://doi.org/10.1016/j.jmrt.2020.12.009

Sharma, P., & Dwivedi, D. K. (2019). A-TIG welding of dissimilar P92 steel and 304H austenitic stainless steel: Mechanisms, microstructure and mechanical properties. *Journal of Manufacturing Processes*, *44*, 166-178. https://doi.org/10.1016/j.jmapro.2019.06.003

Sivakumar, J., Vasudevan, M., & Korra, N. N. (2021). Effect of activated flux tungsten inert gas (A-TIG) welding on the mechanical properties and the metallurgical and corrosion assessment of Inconel 625. *Welding in the World*, *65*(6). https://doi.org/10.1007/s40194-020-01061-4

Suryana, Pramono, A., Muda, I., & Setiawan, A. (2019). The influence of heat input to mechanical properties and microstructures of

API 5L-X65 steel using submerged arc welding process. *MATEC Web of Conferences*, *269*, 1-7. https://doi.org/10.1051/matecconf/2019 26901009

Unni, A. K., & Muthukumaran, V. (2021). Numerical simulation of the influence of oxygen content on the weld pool depth during activated TIG welding. *International Journal of Advanced Manufacturing Technology*, *112*(1-2). https:// doi.org/10.1007/s00170-020-06343-1

Vasudevan, M. (2017). Effect of A-TIG welding process on the weld attributes of type 304LN and 316LN stainless steels. *Journal of Materials Engineering and Performance*, *26*(3), 1325-1336. https://doi.org/10.1007/ s11665-017-2517-x

Vidyarthy, R. S., Dwivedi, D. K., & Muthukumaran, V. (2018). Optimization of A-TIG process parameters using response surface methodology. *Materials and Manufacturing Processes*. https://doi.org/10.1080/10426914. 2017.1303154

Vidyarthy, R. S., & Sivateja, P. (2020). Influence of activating flux tungsten inert gas welding on mechanical and metallurgical properties of the mild steel. *Materials Today: Proceedings*, *28*, 977-981. https://doi.org/10.1016/j.matpr. 2019.12.335

P. Sivateja is a Research Scholar in the Department of Mechanical Engineering, BITS Pilani, Hyderabad campus. He did his graduation from GITAM University and Post graduation from Andhra University, Visakhapatnam. Currently, he is working in the field of Activated tungsten inert gas welding. He has published two technical papers in International conferences/Journals.

Dr. R. S. Vidyarthy is working as an Assistant Professor in the Department of Mechanical Engineering, BITS Pilani, Hyderabad campus. He obtained Ph.D in Mechanical Engineering from the Department of Mechanical and Industrial Engineering, Indian Institute of Technology Roorkee, in 2018. Currently, he is working in welding engineering and wire additive manufacturing to increase fabrication productivity by joining similar and dissimilar metals. He is guiding two Ph.D scholars, published about 17 research papers in journals/ conferences and also has a granted patent on dissimilar steel joining using A-TIG.

(E-mail:ravi.vidyarthyfme@hyderabad.bits-pilani.ac.in)